Primljen / Received: 24.5.2021.
Ispravljen / Corrected: 10.1.2023.
Prihvaćen / Accepted: 22.1.2023.
Dostupno online / Available online: 10.3.2023.

Deformation anisotropy of soft rock

Authors:

Prof. **Slobodan Živaljević**, PhD. CE
University of Montenegro
Faculty of Civil Engineering in Podgorica
slobodanz@ucg.ac.me
Autor za korespondenciju

Prof. **Zvonko Tomanović**, PhD. CE
GeoT d.o.o, Podgorica, Montenegro
zvonko@geot.me

Borko Miladinović, MSc. CE
University of Montenegro
Faculty of Civil Engineering in Podgorica
borkom@ucg.ac.me

Research Paper

Slobodan Živaljević, Zvonko Tomanović, Borko Miladinović

Deformation anisotropy of soft rock

Bedding, being a typical feature of sedimentary rocks, is a cause of inherent anisotropy of deformation properties of rock mass. Results of uniaxial and triaxial, short-term and creep tests conducted by the authors on the specimens of a soft sedimentary rock - marl are presented in this paper. Interpolation of results of the short-term tests enabled for determining the parabolic dependence of secant modulus of deformability on angle (α) between load and natural bedding planes in the interval from 0 to 90 degrees. The time-dependent deformation response is described by determining the dependence of parameters of the modified Wallner's model on the angle α in the interval from 45 to 90 degrees, based on the results of the performed creep tests.

Key words:
soft rock, creep, anisotropy, bedding, secant modulus, triaxial, marl

Prethodno priopćenje

Slobodan Živaljević, Zvonko Tomanović, Borko Miladinović

Anizotropija deformacijskih svojstava meke stijene

Slojevitost kao tipično svojstvo sedimentnih stijena, uzrok je inherentne anizotropije deformacijskih svojstava stijenskih masa. Rezultati jednoosnih i troosnih, kratkotrajnih i testova puzanja provedenih od strane autora na orijentiranim uzorcima meke sedimentne stijene - lapora prezentirani su u ovom radu. Interpolacijom rezultata kratkotrajnih pokusa utvrđena je parabolična ovisnost sekantnog modula deformabilnosti o kutu (α) između opterećenja i ravnine prirodne slojevitosti u intervalu od 0 do 90 stupnjeva. Vremenski ovisan deformacijski odgovor je opisan utvrđivanjem ovisnosti parametara modificiranog Wallnerovog modela o kutu α u intervalu od 45 do 90 stupnjeva na osnovi rezultata provedenih testova puzanja.

Ključne riječi:
meka stijena, puzanje, anizotropija, slojevitost, sekantni modul, troosni, lapor

1. Introduction

The anisotropy of soft sedimentary rock has a significant effect on the stress-strain behaviour during the execution and operation phases of cuts, slopes, tunnels, and other geotechnical structures. The significance of soft rock anisotropy is briefly elaborated using the analysis of the stress state near a tunnel opening, provided its practical importance and characteristics of the secondary stress state induced by the tunnel construction. Excavation of the tunnel opening was followed by a change in the natural primary stress state of the rock mass in the immediate vicinity of the opening. A new stress equilibrium state based on the size of the opening, rock mass properties, and selected support was established. Under the secondary stress state, some rock elements undergo unloading in the radial direction, whereas other elements undergo additional loading in the tangential direction, as shown in Figure 1. The load redistribution induced by the excavation of the opening was followed by the instantaneous occurrence and development of time-dependent deformations. Prediction of the overall deformation response of the surrounding rock mass of the circular opening is of key importance to the tunnel design and construction. The estimation of time-dependent deformation (creep) is particularly important for soft rocks, such as rock salt, marl, claystone, and mudstone, because the value of time-dependent deformations can achieve the value of instantaneous deformations depending on the time interval between the excavation phases. In addition, creep deformation can lead to a higher time-dependent pressure acting on the supporting structures [1].

In general, all rock masses are naturally anisotropic owing to the presence of cracks, faults, and other secondary structures. However, even intact rocks can be anisotropic as a result of their genesis; indeed, they have some primary structures, such as layering, schistosity, lamination, and foliation. Furthermore, this inherent anisotropy is also a characteristic of metamorphic and sedimentary rocks. In addition, isotropy may be induced by a change in the stress state [2]. However, the subject of this study was the inherent anisotropy of deformable properties of sedimentary rocks.

Bedding is a typical feature of sedimentary rocks and causes inherent anisotropy in the deformation properties of rock masses. The mechanical behaviour of most natural deposits is anisotropic because of the anisotropic microstructure formed during the sedimentation process [3]. In this study, bedding refers to a typical favoured orientation of mineral particles in the horizontal planes perpendicular to the direction of sedimentation resulting from the deposition, compaction, and diagenesis conditions of rock. Transverse isotropy is a type of anisotropy, which is defined by one plane of isotropy, that is, bedding plane, and an axis of anisotropy normal to the bedding plane, that is, the direction of sedimentation [4, 5]. In general, the effects of transverse and anisotropy on the strength has been extensively researched [6-10] unlike the effects of anisotropy on the instantaneous and time-dependent deformations in particular.

Figure 1 illustrates the typical prismatic elements of sedimentary rock around the tunnel opening, which are loaded or unloaded perpendicular to the bedding plane, parallel to the bedding plane, and at an angle of 45° to the natural bedding plane within the total distribution of secondary stresses. Instantaneous deformation modulus, which is perpendicular to the bedding plane, is usually higher than the deformation modulus parallel to the bedding plane [11]. Nasseri et al. used the results of uniaxial and triaxial tests to determine the change in the tangent modulus of elasticity for schist depending on the angle between the loading and bedding planes (α) [12]. A decreasing trend in the modulus of elasticity with an increase in the angle was determined by Meng [13] for sandstones and Jin [14] for shale. Moreover, the velocities of secondary creep in the case where the specimen is loaded perpendicular to the bedding plane are generally greater than that where the specimen is loaded parallel to the bedding plane [15-20]. Therefore, for both the short- and time-dependent cases, the deformation response of certain rock elements near the tunnel opening depends on the loading/unloading orientation angle to the natural bedding plane.

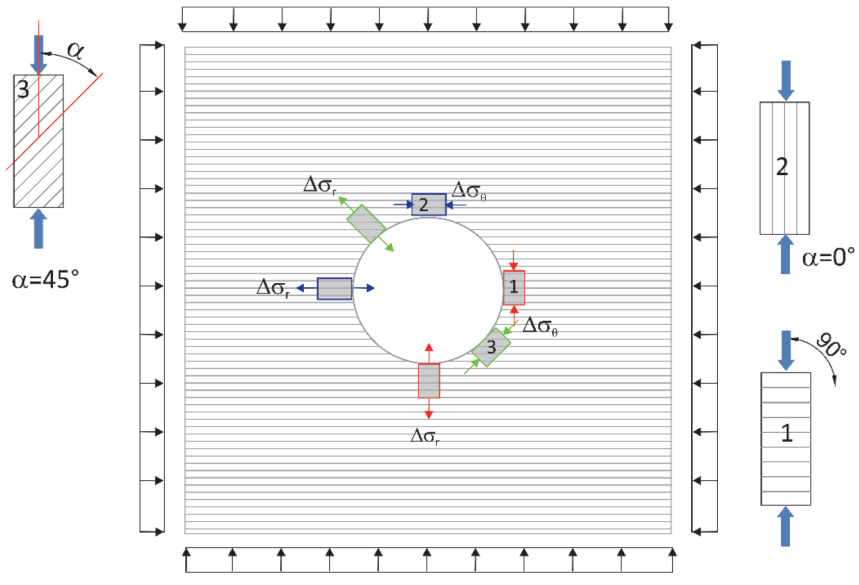

Figure 1. Secondary state of stress around circular tunnel opening

In contemporary design practices, the typical computation of supporting tunnel structures involves the FEM/FDE methods implemented in commercial software packages based on the selected rheological model. Therefore, the applied rheological model should ideally include the short- and long-term behaviours of rock under loading and unloading conditions, and inherent anisotropy

of the rock. However, regardless of the availability of more advanced models, isotropic models are still commonly used in practice. Indeed, nonlinear models have different material properties under loading/unloading conditions. Li et al. developed a viscoelastoplastic model for a bedded argillaceous rock [21]. Wang et al. proposed a viscoplastic model for modelling the transversally isotropic behaviour of carbonaceous slate [22].

This study presents the selected experimental results on the instantaneous and time-dependent deformation response of Neogene marl as a representative of soft sedimentary rocks. This study is part of an extensive research on the Neogene marl that was carried out at the Faculty of Civil Engineering in Podgorica in two experimental campaigns conducted in 1999 to 2004 and 2011 to 2015. The first campaign focused on the loading deformations of prismatic and plate specimens, whereas the second campaign investigated the unloading creep deformation. A limited number of specimens that were not tested during the second campaign were employed to explore the effects of material anisotropy on the short- and long-term deformations of the material using short- and long-term uniaxial and triaxial tests at different bedding planes' orientations in relation to the loading direction.

This study describes the properties of material, preparation of specimens, testing equipment, and test procedures, and presents the characteristic results. The deformation response is described by determining the correlation between the parameters of the modified Wallner's model (creep-related) and the angle α in the range of 45 to 90° based on the results of the conducted tests. The short-term response is described by determining the correlation between the secant modulus of deformability and angle α. The distinctive nonlinear response of the material requires the use of secant models. The applied methodology interpolates the uniaxial creep test results to determine the correlations in the uniaxial stress state at the specimen orientation angles of 0, 45, and 90°. However, a considerably more extensive scope of tests compared to those used in this study is required to explore the effect of lateral stress on the model.

2. Experimental study

2.1. Material properties

The source of marl specimens is the open pit Potrlica in the Pljevlja Basin, as shown in Figure 2, Montenegro, which is a shallow paleokarst depression filled with coal-bearing sediments deposited during the Miocene, during which this area was occupied by the Lake of Pljevlja. The marls found in the Pljevlja Basin are lake sediments of Miocene age, which make the overlying roof of the main coal layer along with the marl limestone. The Pljevlja Basin belongs to the youngest Lower Miocene, approximately corresponding to the upper Carpathian. The chemical analysis and determination of microflora and microfauna have revealed that the Lake of Pljevlja belonged to the type of hydrologically open carbonate hard-water lakes. In this lake type, runoff and evaporation are at equilibrium with the water inflow. According to the Wright classification, it is a low-energy lake with a steep shore (in Potrlica), defined by pre-Miocene faults [23]. Moreover, the area of Potrlica belongs to the profundal zone of Neogene Lake in Pljevlja.

The sediment thickness increased from the brim towards the centre of the basin, where the thickness was 128 m. The layers can be classified in four levels-packages based on the content of calcium carbonate: the first 25 m above the coal layer contains 90 % $CaCO_3$ (marl limestone), the subsequent 30–40 m is a cement marl layer (70 % $CaCO_3$), overlaid with a layer of approximately 20 m of marl limestone (90 % $CaCO_3$), which is underneath the top layer made of cement marl with a thickness of 40–50 m (70–75 % $CaCO_3$).

Pettijohn reported that marl is defined as a rock with 35–65 % of carbonate and complementary clay content [24]. The scanning electron microscopy (SEM) images of natural tested marl revealed heterogeneous porous mixture of carbonate grains and clay particles, as shown in Figure 3.

According to X-ray diffractometry, as illustrated in Figure 3.b, the tested marl is mainly composed of calcite (64.4 %) and quartz (8.3 %), whereas the clayey phase includes illite (6.3 %), montmorillonite (9.6 %), and muscovite (11.3 %). Moisture of the tested specimens was in the range of 16–19 %, and average uniaxial compressive strength of the material was approximately σ_c = 11.65 MN/m^2. The dependence of uniaxial compression strength (UCS) of the cylindrical and prismatic marl specimens when loaded at angles of 0, 45, and 90° in relation to the natural bedding plane is illustrated in Figure 4. Despite the significant scattering results, the natural moisture content evidently affected the obtained uniaxial compressive strength values in relation to the specimen orientation and dimensions. In terms of weathering, pursuant to the ISMR classification [25], the tested specimens were assigned

Figure 2. Open pit Potrlica of the coal mine in Pljevlja, Montenegro

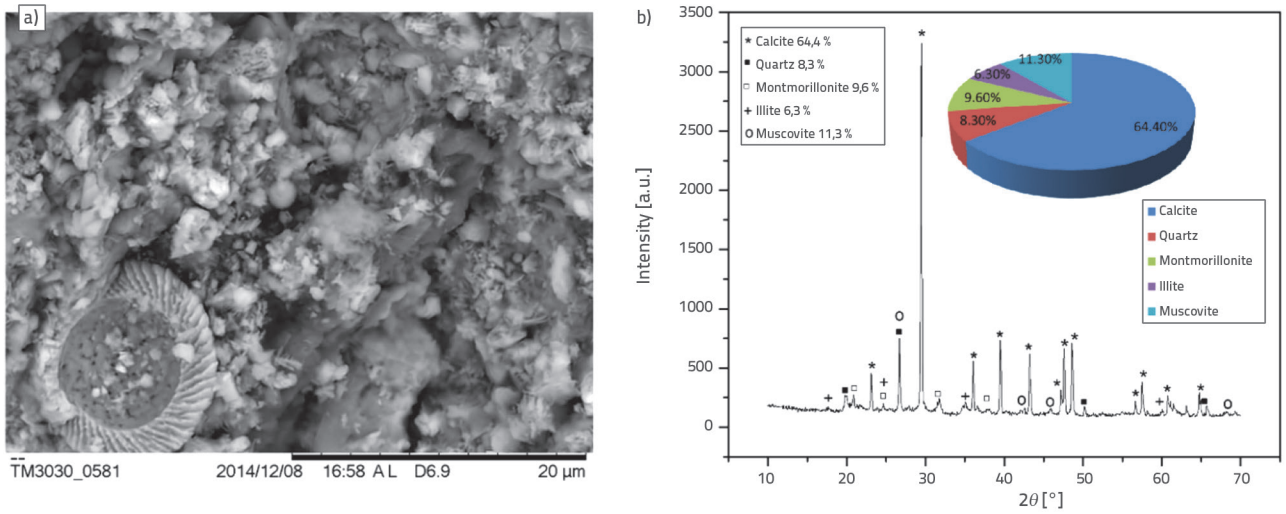

Figure 3. a) SEM images of tested marl at a magnification of 5000x ; b) mineral components through X-ray diffraction

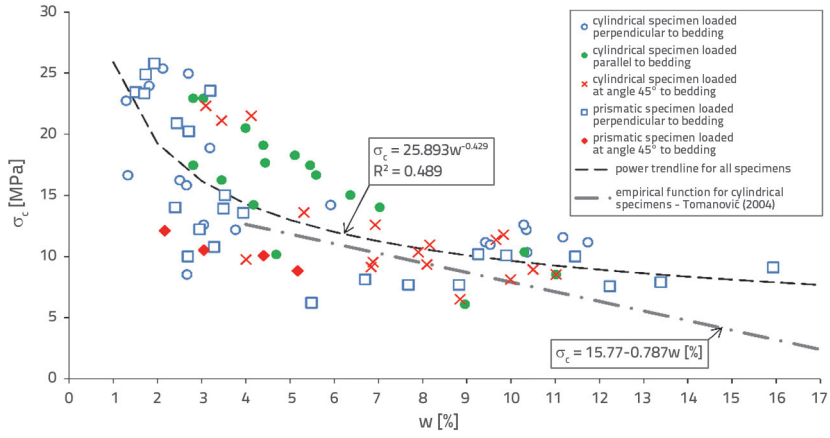

Figure 4. Uniaxial compressive strength of marl specimens as a function of moisture content

grade F for fresh rock with no visible signs of rock material weathering.

2.2. Preparation of specimens

A relatively compact marl block was extracted from one bench of the open-pit mine at a depth of approximately 20 m from the actual terrain surface and transported to a stone cutting plant, as shown in Figure 5.a, where a plate with a thickness of 15 cm was cut out, as shown in Figure 4.b. Prismatic specimens with a width/length/height of 15/15/40 cm were cut from each plate, packed, and transported to the laboratory, as shown in Figures 5.c and d. In general, sampling, transport, processing, and storage of specimens before and during the testing processes were performed with a reasonable care to prevent an increase in the degree of weathering to the extent that could affect the strength, and short- and long-term deformations. Immediately after sampling in mid-September 2010, the blocks were transported to a covered facility and protected using a plastic wrap. In September 2010, the block was delivered to a stone cutting factory in Danilovgrad. Water jet cutting did not degrade the specimens; however, it caused a shallow penetration of water in the specimen. After cutting, the specimens were dried for several days until the natural moisture content recovered at a rate that did not cause degradation even in the surface zone. One part of the specimen was immediately tested to determine the chemical and mineralogical composition and the correlations between the UCS and water content, specimen shape, and load orientation. After moisture control, most specimens were packed such that they were stored without any significant loss of moisture over a long period. In addition, the specimens were stored at a room in which the air humidity could not significantly vary during the year with seasonal temperature changes.

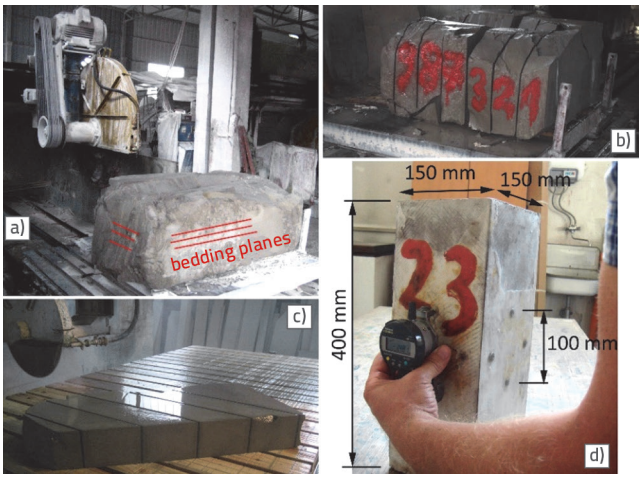

Figure 5. Preparation of prismatic marl specimens for the uniaxial creep test

Immediately before testing, the prismatic specimens were equipped with measurement points used to measure the deformation in the direction of the longitudinal axis of the specimen (axial and vertical) and horizontal deformations, as shown in Figure 5.d. The measurement base had a thickness of 100 mm. A digital comparator was used in the measurements, as presented in Figure 5.d. The steel measurement points were affixed to the specimens using an epoxy adhesive, based on a grid previously drawn on the surface of the specimens. Thereafter, the specimens were coated with a thin layer of hot paraffin to reduce the moisture loss during the test period. The same method was applied to prepare non-loaded prismatic specimens (the so-called compensation prisms) for monitoring deformations resulting from temperature and moisture content changes, which generally shrink the specimens without a stress change, yet at higher temperatures and relative elongation of the specimens, as shown in Figure 7.

Cylindrical specimens were cut out from the previously prepared specimens in a cube shape of 15 cm x 15 cm x 15 cm, using a rotary cutting machine in the laboratory of the Faculty of Civil Engineering, as shown in Figure 6.a. The specimens were cut perpendicular to the natural bedding plane at an angle of 45°, and parallel to the bedding orientation. The specimens had a diameter and height of 56 and 108 mm, respectively. The specimens were cut to a proper length using a rotary blade cutting machine in the laboratory of the Faculty of Civil Engineering, where the bases of the specimens were polished.

In the conventional triaxial test, cylindrical specimens were equipped with strain gauge rosettes to measure the deformations in two mutually perpendicular directions (type FCA-10-11, gauge length 10 mm, manufacturer TML, Japan). Three rosettes were attached to each specimen, positioned at the mid-height of the specimen, and arranged at equal distances according to the specimen volume, as shown in Figure 6.b. Moreover, a two-component P-2 (TML) adhesive was used. The cable connecting the rosette to the data logger was assumed to be as thin as possible because of the limited space in the Hoek triaxial cell. A piece of ribbon cable was connected to the rosette of the specimen and continued as a regular outlet cable at the cell exit. Subsequently, the specimen was placed on a protective membrane (ELE, UK). Triaxial creep tests conducted on the trial series of specimens revealed that the specimens equipped in this manner enabled the monitoring of time-dependent deformations over a period of several months.

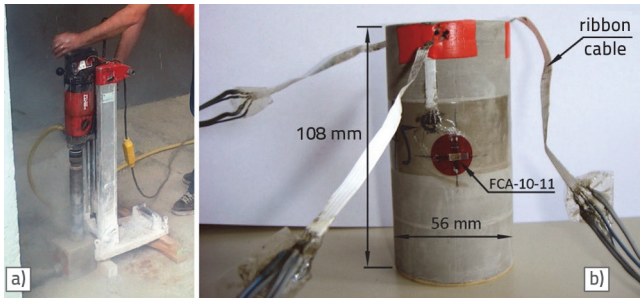

Figure 6. Preparation of cylindrical marl specimens

Considering the air humidity and temperature variations over the course of multiannual testing, as presented in Figure 7.a, compensation (non-loaded) prisms identical to those tested were placed close to the testing device. Each measuring of deformations in the loaded prisms at the same time included measuring of deformations in the compensation prisms 46, 73, and VIII, as shown in Figure 7.b, to correct measurement results owing to the effect of the air temperature/humidity in the laboratory. Thus, the effect of these two variables on the shrinkage/expansion of the specimens was eliminated by determining the total measured deformation during the creep test. This allowed the isolation of the creep deformation from the total measured deformation.

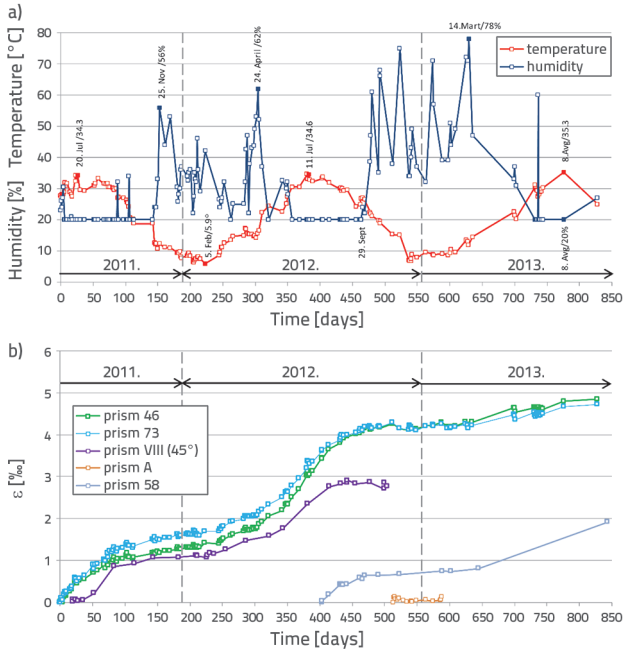

Figure 7. Comparison of: a) the air temperature and humidity in the laboratory; b) axial deformations of the compensation prisms

2.3. Description of equipment and testing procedure

A double-lever arm device with a capacity of 750 kN, as presented in Figure 8.a, was used to maintain a constant axial stress on the specimens. The device was readjusted to enable the simultaneous testing of three prismatic specimens of the same series by placing the specimens on top of each other [26]. A weight was hung at the end of lever arm 2, transferred to lever arm 1, and applied to the specimen as a compressive stress. Depending on the position of the specimen along the lever arm 1, the hanging weight was multiplied by 10 to 150 times. A previously designed proving ring device with a capacity of 250 kN, as shown in Figure 8.b, was used to measure the applied load and load control during the creep test. The advantage of using a mechanical system is that long creep test durations in the order of years can be achieved in comparison

to conventional hydraulic servo-loading systems. Lu and Wang developed a similar cantilever-type multi-arm lever device for the creep testing of mudstone [27].

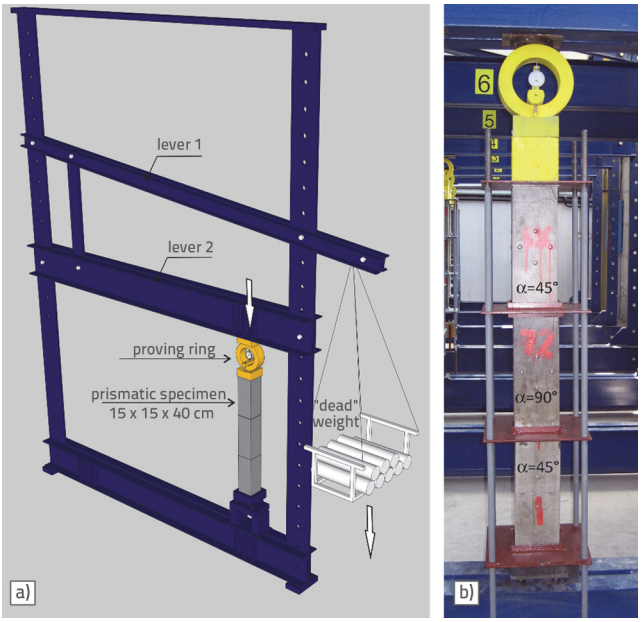

Figure 8. Testing equipment: a) double-lever arm device; b) frame PR-7

The axial load was applied in increments of value equal to the one fourth of the total stress in the creep test. Deformations were measured after 15, 30, 45 min, and 1, 3, 6, 12, and 24 h, and 3, 7, and 15 d following the loading, and once a month subsequently. During the deformation measurements of the loaded specimens, the deformations of two unloaded specimens were also measured to determine the deformations stemmed from changes in the moisture content, shrinkage in the specimen, and ambient temperature, that is, temperature and humidity correction. Additionally, one specimen in the series PR-7 (prism 72) was prepared by cutting perpendicular to the bedding plane for comparison purposes, as shown in Figure 8.b.

In the triaxial creep tests, three adjacent double-lever arm devices (frames 4, 5, and 6) were arranged, as illustrated in Figure 9. A hydraulic cylinder with a capacity of 50 ton was mounted on frame 4, whereas a Hoek triaxial cell was mounted on frames 5 and 6. The hydraulic cylinder, two cells, a manometer, and a pressure gauge were connected to a single system using flexible hoses. After the non-return valve, the oil hose from the cylinder runs in branch lines toward the manometer and cell no. 1, which is connected to cell no. 2, as shown in Figure 10.b; subsequently, a line running toward the pressure gauge connected to the data logger exists. The pressure gauge is a TML pressure transducer with the capacity of 20 MPa and accuracy of 0.01 MPa, as presented in Figure 10.a. Air valve of the pressure gauge, as illustrated in Figure 10a, was used not only to release the residual air remaining after the cell filling with oil but also to occasionally drain oil to maintain a relatively constant cell pressure.

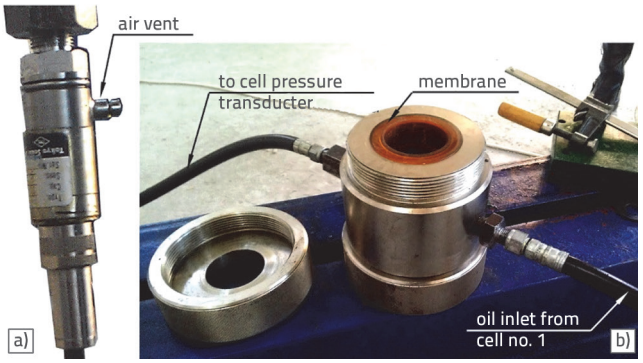

Figure 10. Details of the arrangement for the triaxial creep test: a) pressure gauge – TML cell pressure transducer, b) Open triaxial cell no. 2

This arrangement enabled the application of a load and maintained the same value of oil pressure in the triaxial cells, that is, simultaneous testing of two specimens in one series under the same lateral stress. Compared to the creep test performed on the prismatic specimens, the specificity of this test is reflected in the method of applying the axial load. This particular test imposes the application of lower axial force values for the same required level of axial compression because of various specimen sizes. Provided that the dead weights of levels 1 and 2 exceeded the required load, the frames were fitted with a mechanism that helps reduce the weight to the required value. A rope was run over a hook pulley with one rope end tied to lever 1 and a basket with dead weight hanging from the other rope end. The added weight was expected to lift lever 1, indicating unloading and further implying that the process of applying the axial force removes parts of the load.

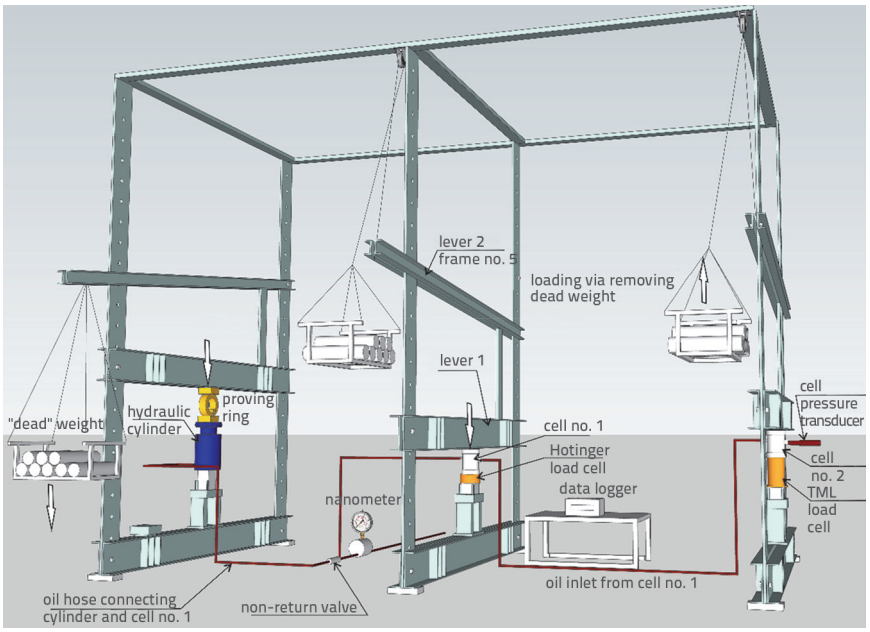

Figure 9. Frame arrangement in the triaxial creep test

3. Selected results of the short-term tests

This section presents the characteristic results of short-term uniaxial and triaxial tests performed on the oriented cylindrical marl specimens. Uniaxial tests were performed on two cylindrical specimens with different orientations ($\alpha = 0$ and $90°$) under identical moisture contents. Following the first unloading, additional three ($\alpha = 90°$), that is, four ($\alpha = 0°$) unloading-reloading cycles, were performed. Diagrams of the average axial and radial deformations as functions of axial stress are illustrated in Figures 11 and 13. In general, the stress-strain curves indicate the nonlinearity of the material, accumulation of reversible deformations after each cycle, and hysteresis in the unloading-reloading cycle.

For the specimen loaded perpendicular to the bedding, the secant moduli of deformability, as shown in Figure 12, at a loading within one cycle initially increased, that is, concave upward curve in Figure 11, and then decreased with an increase in the axial stress, as presented in Figure 10. This behaviour is attributed to the closure of contacts of the bedding planes under a load perpendicular to them. Furthermore, this hypothesis is supported by the decreasing trend of the secant modulus observed in the specimens loaded parallel to the bedding planes within one loading cycle, as shown in Figure 14. An increasing trend in the modulus of deformability throughout the cycles was observed for both tested specimens. This trend is more distinct in specimens where $\alpha = 90°$ and can be explained by hardening (pre-consolidation) of the material in the previous cycle.

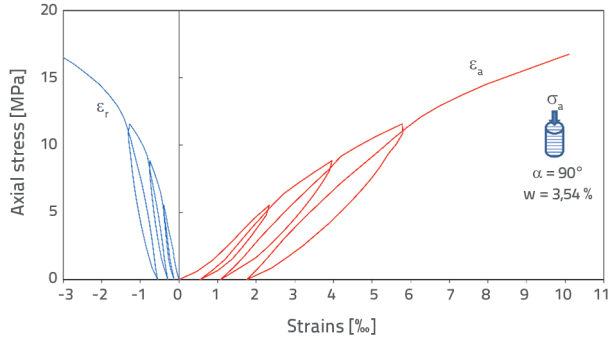

Figure 11. Axial and radial deformations of specimen loaded perpendicular to the bedding plane

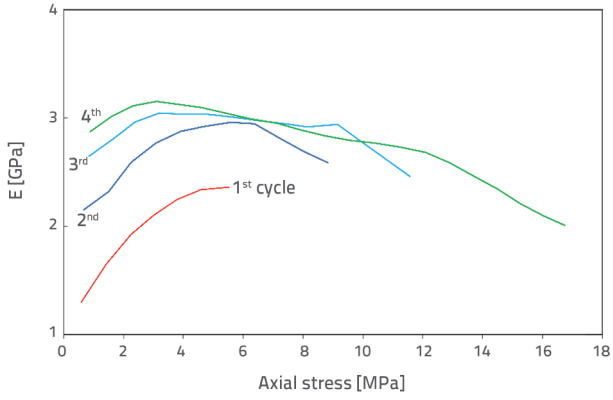

Figure 12. Secant moduli of deformability as measured perpendicular to bedding for different loading cycles

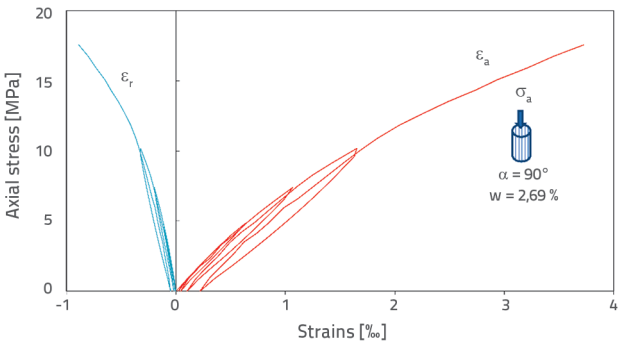

Figure 13. Axial and radial deformations of specimen loaded parallel to bedding planes

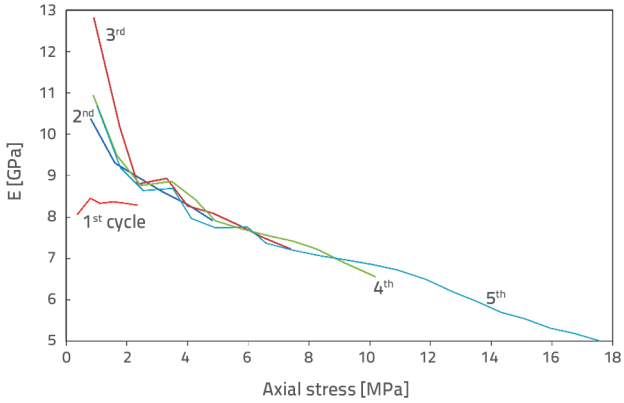

Figure 14. Secant moduli of deformability as measured parallel to bedding for different loading cycles

Figure 15 shows the characteristic results of the conventional triaxial compression test performed on the specimens that were loaded axially perpendicular to the bedding for the two levels of lateral stress. Figure 16 shows the secant moduli of deformability as a function of the axial and lateral stresses. Values of the secant moduli increase with an increasing lateral stress. Furthermore, compared with the uniaxial test (p = 0.0 MPa), the presented curves indicate only a decrease in the secant modulus with an increase in the axial stress.

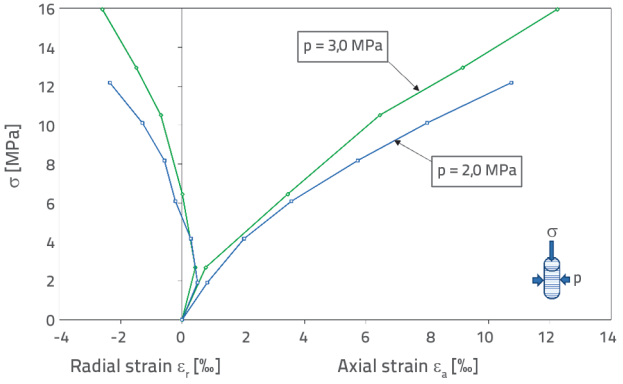

Figure 15. Axial stress-strain of the specimen loaded perpendicular to the bedding plane for two levels of lateral stress

The secant moduli measured using triaxial tests at angles of 0, 45, and 90° with respect to the axial–lateral stress relation σ/p are shown in Figure 17. Values of the lateral stress in tests were 2.0 and 3.0 MPa. The dashed lines indicate the dependence of the secant moduli on σ/p obtained using the regression analysis. Despite the evident scattering results, the obtained dependences were used to estimate the relative relationships between the moduli for the three angles, as shown in Figure 18. The average relationship values of the secant moduli of deformability were E^0/E^{90} = 2.88 and E^{45}/E^{90} = 1.50.

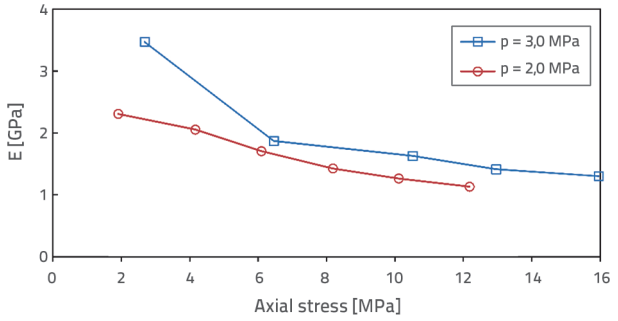

Figure 16. Secant moduli of deformability as measured perpendicular to bedding for two levels of lateral stress

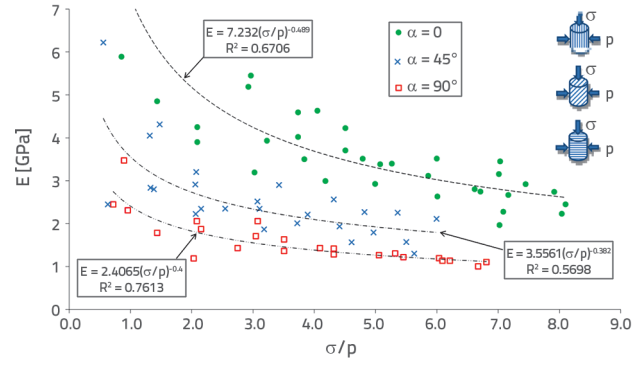

Figure 17. Secant moduli as a function of angle α, dashed lines are the regression curves

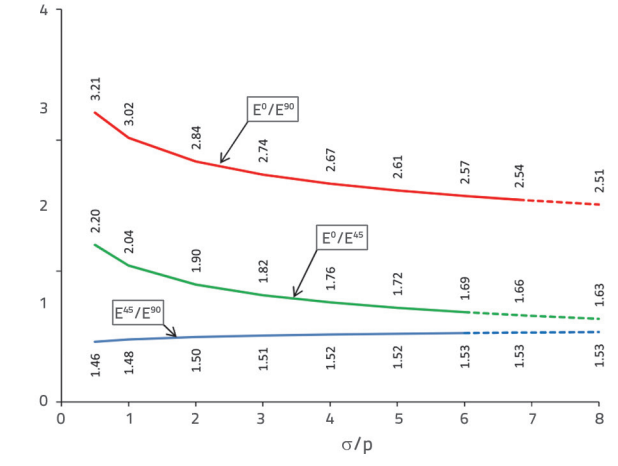

Figure 18. Relationship between secant moduli

4. Selected results of the creep tests

4.1. Uniaxial creep tests

Uniaxial creep tests were performed on two series of three prismatic specimens (PR-7 and PR-8) for a creep stress level of 2.0 MPa for a duration of one month and 4.0 MPa for four months. One specimen in series PR-7 was perpendicularly loaded to the bedding, and other specimens were loaded at an angle of 45°. Subsequently, the measured average moisture content was 3.4 %, and the average uniaxial compressive strength was 10.38 MPa. The instantaneous response of the material to the applied creep stress is expressed by the secant moduli of deformability; Table 1 lists the average values the secant modulus of deformability of marl.

Table 1. Average values of the secant modulus of deformability of marl

σ [MPa]	2.0	4.0
E^{90} [GPa]	1.21	1.91
E^{45} [GPa]	2.23	3.03
E^{45}/E^{90}	1.84	1.59

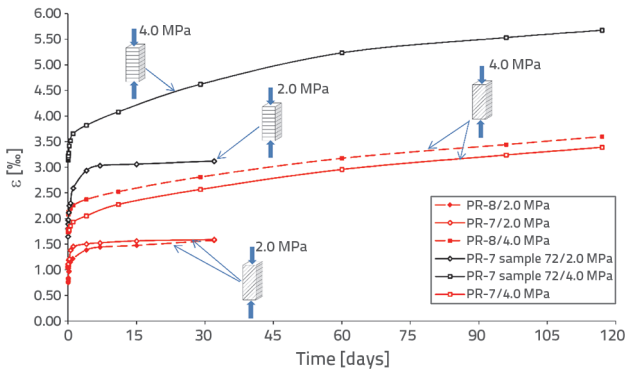

Figure 19. Creep test results for PR-7 and PR-8. Comparison of total axial deformations at stress levels of 2.0 and 4.0 MPa

Figure 19 shows a comparison of the total axial deformations and Figures 20 and 21 present the creep deformations that indicate the development of primary and secondary creeps, respectively. For both levels of axial stress, the creep deformations of specimens loaded at an angle of 45°, $\varepsilon_a(45°)$ in relation to the natural bedding were lower than those of the specimen loaded perpendicular to bedding $\varepsilon_a(90°)$. Hence, for the stress level of 2.0 MPa, the relationship of the average axial deformations was $\varepsilon_a(90°) / \varepsilon_a(45°) = 2.15$ after approximately one month, whereas it was 1.61 after four months at the stress level of 4.0 MPa. As shown in Figure 22, the comparison diagrams of the average deformation rates suggest that the primary and secondary creep rates were generally higher for specimens loaded perpendicular to the bedding. After 20 days, the relationship between the creep rates perpendicular to and

at an angle of 45° from the bedding was 1.88 at a creep stress of 4.0 MPa. Approximately 2.5 months after the beginning of the test, this relationship was approximately 1.00.

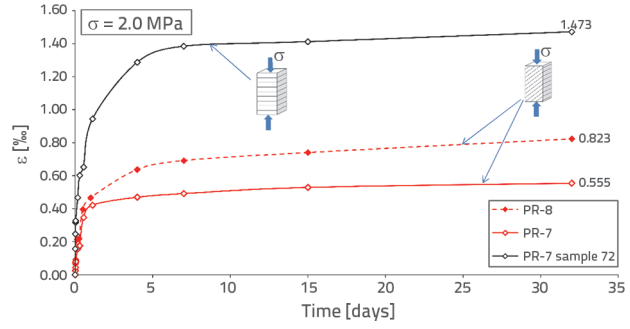

Figure 20. Comparison of axial creep strains at axial stress level of 2.0 MPa for PR-7 and PR-8

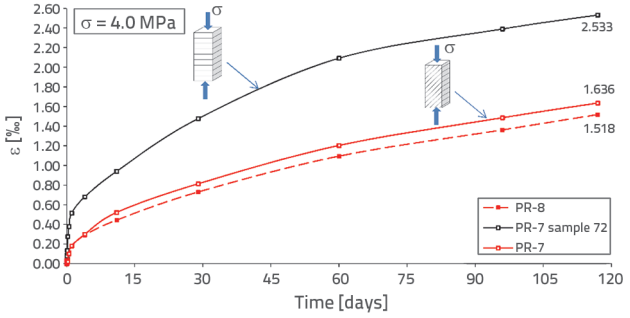

Figure 21. Comparison of axial creep strains at axial stress level of 4.0 MPa for PR-7 and PR-8

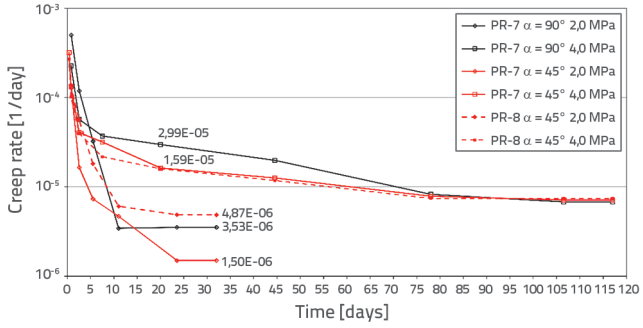

Figure 22. Comparison of creep rate for the creep stress levels of 2.0 and 4.0 MPa

4.2. Results of the triaxial creep tests

In the triaxial creep tests, two specimens were examined with axial loads perpendicular to the bedding planes, and two specimens with axial loads parallel to the bedding planes. In the first phase of the tests, the specimens were exposed to a constant stress deviator of 1.0 MPa (lateral stress = 1.0 MPa, axial stress = 2.0 MPa) over 28 and 25 days, respectively. The next phase involved total unloading and measurement of the reversible deformation over 28 and 25 days. Figure 23 shows total axial and radial deformations over time for the specimens subjected to an axial stress perpendicular to the bedding (α = 90°). Figure 24 shows total axial and radial deformations over time for the specimens subjected to an axial stress parallel to the bedding (α = 0°). The axial deformations prove the development of primary and secondary creeps and radial deformations show similar tendencies. The average rate of the secondary creep in the axial direction was $5.10 \cdot 10^{-6}$ / day for an axial load perpendicular to bedding, whereas it was $2.67 \cdot 10^{-6}$ / day for an axial load parallel to bedding (rate = 1.91). The ratio of the achieved axial creep strains over a period of 25 d, ε_{cr} (90°) / ε_{cr} (0°), was approximately 2, as shown in Figure 25. The ratio of the total radial and axial strains practically remained constant during the creep test, as shown in Figure 26. However, the average ratio $\varepsilon_r/\varepsilon_a$ is higher at α = 0° (0.38) than that of α = 90° (0.167) because the radial stress at α = 0° acts perpendicular to the bedding plane.

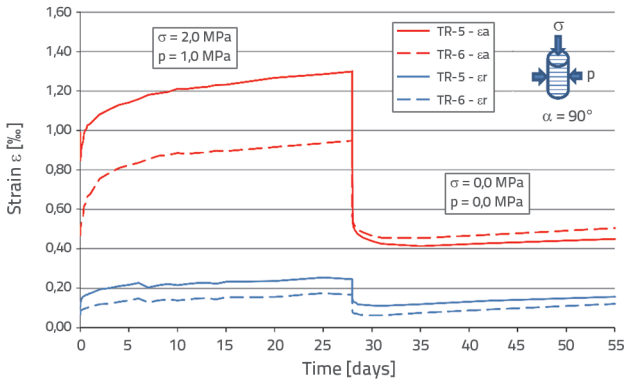

Figure 23. Total axial and radial strains on the specimens loaded perpendicular to bedding planes

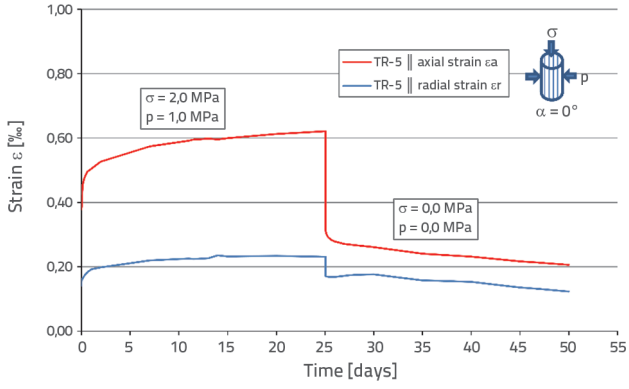

Figure 24. Total axial and radial strains on the specimens loaded parallel to bedding planes

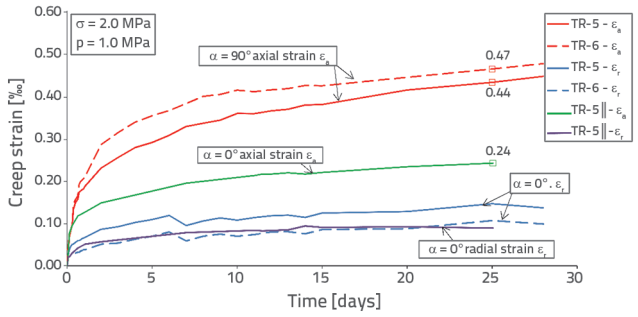

Figure 25. Comparison of axial and radial creep strains at α = 0 and 90°

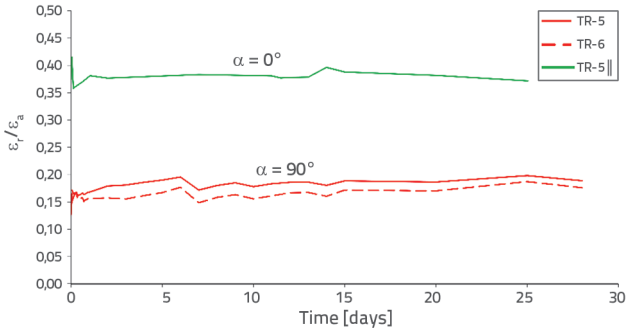

Figure 26. Ratio of total radial and axial strains during the creep test

5. Material constitutive model

The instantaneous deformation response of marl can be described by its secant modulus of deformability. Experimental evidence indicates the nonlinear behaviour and dependence of the secant modulus on the level of axial stress, level of lateral stress, and angle α, as illustrated in Figure 27.a at p = 3.0 MPa. For a fixed value of the lateral stress, the dependence of the secant modulus on the angle α and ratio σ/p can be approximated using the following function:

$$E(\sigma/p, \alpha) = k_1(\sigma/p)\alpha^2 + k_2(\sigma/p)\alpha + k_3(\sigma/p) \quad (1)$$

where $k_1(\sigma/p)$, $k_2(\sigma/p)$, $k_3(\sigma/p)$ were interpolated using a sixth-degree polynomial in the interval σ/p from 1 to 7, as shown in Table 2 and Figure 27.b. The diagrams of function E are represented by dashed lines in Figure 27.a, as expressed in Equation (1).

The results of the creep tests indicate that the time-dependent response of marl includes primary and secondary creep strains, which occur when the stress level is below the yield strength ($\sigma < \sigma_F$, Figure 28.a). In this case, the total strain is the sum of the elastic strain and strains of the primary and secondary creep.

$$\varepsilon = \varepsilon^{el} + \varepsilon^{p} + \varepsilon^{s} \quad (2)$$

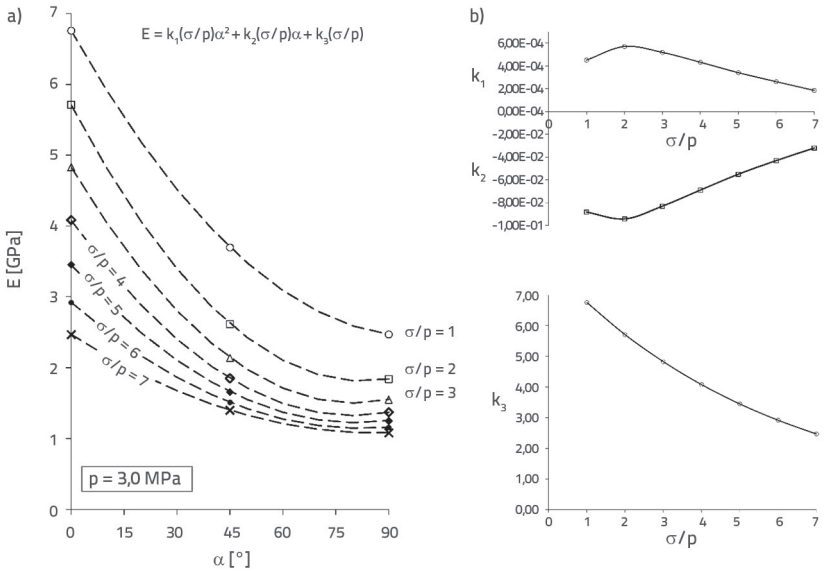

Figure 27. Approximation of the secant modulus of deformability

where:
- ε^{el} - the elastic strain (induced by stress change)
- ε^{p} - the primary creep strain (delayed elasticity)
- ε^{s} - the secondary creep strain.

A modified Wallner's model was used to describe the behaviour of the tested marl under a long-term loading. Wallner's model [28] that was originally developed for rock salts, was modified by Tomanovic [29, 30] based on experimental studies on the marl creep. Mechanical scheme of the modified Wallner's model, as illustrated in Figure 28.b, includes five rheological bodies; the following bodies are relevant to the modelling of the axial creep test results.

Table 2. Interpolating polynomials of functions *a, b,* and *c*

a	$-0{,}000249+1{,}2525833\cdot10^{-3}x-7{,}3844444\cdot10^{-4}x^2+2{,}214375\cdot10^{-4}x^3-3{,}7923611\cdot10^{-5}x^4+3{,}4791667\cdot10^{-6}x^5-1{,}3194444\cdot10^{-7}x^6$
b	$-0{,}018632-0{,}13109243x+0{,}082728169x^2-0{,}025330938x^3+4{,}3864653\cdot10^{-3}x-4{,}40462917\cdot10^{-4}x^5+1{,}5365278\cdot10^{-5}x^6$
c	$8{,}14-1{,}6546667x+0{,}35652778x^2-0{,}098541667x^3+0{,}018402778x^4-0{,}0017916667x^5-6{,}9444444e\cdot10^{-5}x^6$
where $x = \sigma/p$	

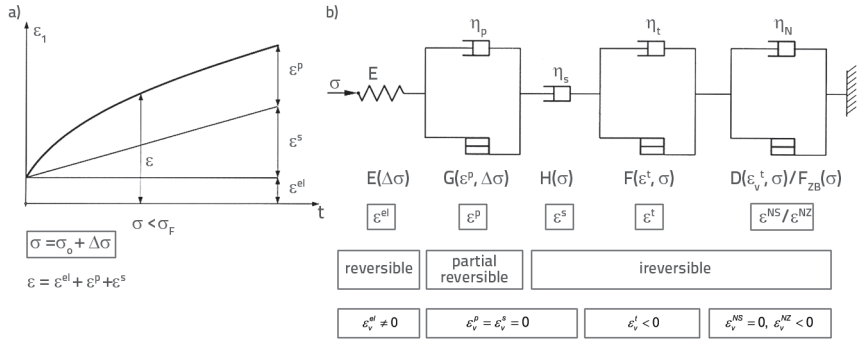

Figure 28. a) Time-dependent deformations after loading, when the stress state is below the yield condition; b) modified Wallner's rheological model

A spring represents an instantaneous deformation response to a stress change. Depending on the actual deformation response of the rock, elastic modulus or modulus of deformability can be used as a nonlinear elastic material.

The parallel relationship between the viscous body and slider represents the primary creep (delayed elasticity), that is, viscoplastic deformation with a strain hardening. This component has the same sign as the instantaneous deformation and depends on the stress change. The primary creep strain was partially reversible. The threshold stress, at which the viscous element was activated, was below the yield strength (plastic limit).

A Newtonian fluid describes the secondary creep. This deformation component depends on the current stress state, which is irreversible.

Modified Wallner's model for the uniaxial loading case can be expressed as

$$\varepsilon = \frac{1}{E(\sigma_1)}\sigma_1 + \frac{3}{2}\left(\frac{\Delta\sigma_1}{E_p}\right)^m \cdot \left(1 - e^{-\frac{2E_p}{3\eta_p}t}\right) + a(\sigma_1)^n t \quad (3)$$

where:

- $E(\sigma_1)$ - the secant modulus of marl deformability
- σ_1 - the axial stress
- $\Delta\sigma_1$ - the stress difference
- E_p - the strain-hardening modulus
- η_p - the viscosity (for the primary creep)
- m - the stress exponent (for primary creep)
- a - the creep parameter
- n - the normalized stress exponent for secondary creep.

The first term in Equation (3) describes the elastic deformation, the second term refers to the deformation of the reversible primary creep, and the third term denotes the deformation of the secondary creep.

The material parameters related to creep, E_p, m, η_p, a and *n* are defined using the least-squares fitting method. The Excel Solver tool was used to minimise the sum of least squares errors. The process used the values of the secant moduli of deformability listed in Table 4. The obtained values of the model parameters for the case of the load applied perpendicularly and at an angle of 45° in relation to the natural bedding planes are presented in Table 3. The total axial deformations measured during the creep tests and the corresponding theoretical curves according to the modified Wallner's model are illustrated in Figures 29 and 30.

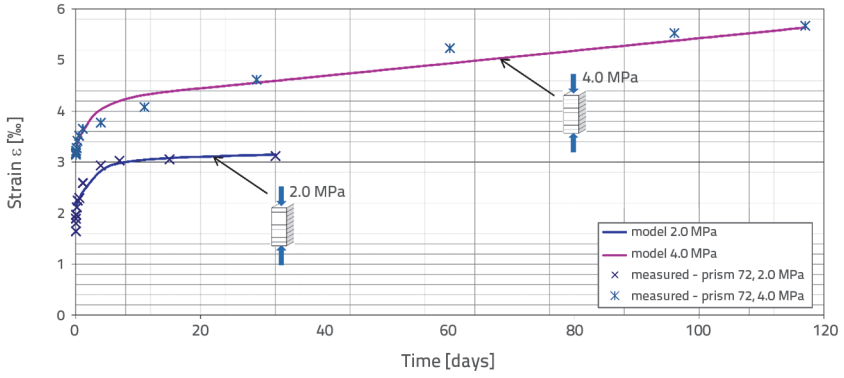

Figure 29. Total deformations of the prismatic specimens of marl (α = 90°) as at stress values of 2.0 and 4.0 MPa (dotted marks) and theoretical curves of marl deformations according to the modified Wallner's model (solid lines)

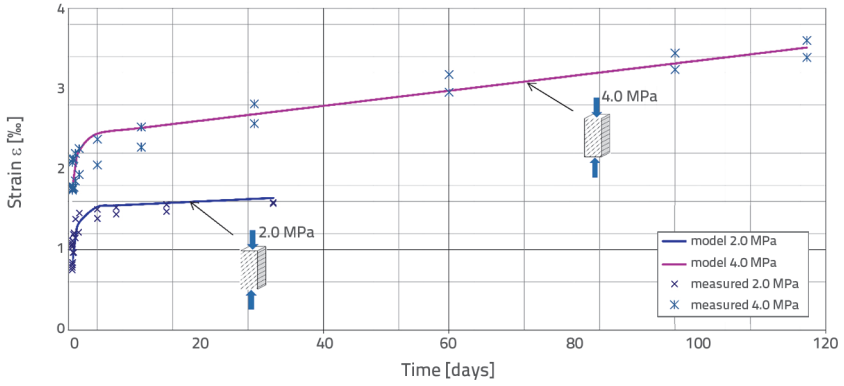

Figure 30. Total deformations of the prismatic specimens of marl (α = 45°) at stress values of 2.0 and 4.0 MPa (dotted marks) and theoretical curves of marl deformations according to the modified Wallner's model (solid lines)

Table 3. Values of material parameters of marl of the primary and secondary creeps after unloading

Parameters	Primary creep			Secondary creep	
	E_p [MPa]	μ_p [MPa·d]	m	a [1/d]	n
Loading perpendicular to bedding	500	600	0.065	0.00120	1.75
Loading at angle of 45° to bedding	700	400	0.010	0.00145	1.35

Table 4. Values of secant modulus of deformability of marl for defining the parameters of primary and secondary creeps

Characteristic stress [MPa]	2.0	4.0
E [GPa]	0.98	1.27
E_{45} [GPa]	2.45	2.35

The equations for creep-related parameter changes of the model in the interval of angles from 45 to 90° can be obtained by linear interpolation of the values listed in Table 3:

$$\begin{aligned} E_p &= 4.44\alpha + 300 \\ m &= 0.001222\alpha - 0.045 \\ \eta_p &= -4.44\alpha + 800 \\ a &= -5.55556\cdot 10^{6}\alpha + 0.0017 \\ n &= -0.00889\alpha + 2.15 \end{aligned} \quad (4)$$

Equation (3) can have the following form using Equations (1) and (4).

$$\varepsilon = \frac{1}{E(\sigma_1 / p,\alpha)}\sigma_1 + \frac{3}{2}\left(\frac{\Delta\sigma_1}{E_p(\alpha)}\right)^{m(\alpha)}\left(1 - e^{-\frac{2E_p(\alpha)}{3\eta_p(\alpha)}t}\right) + a(\alpha)\sigma_1^{n(\alpha)}t \quad (5)$$

The use of Equation (5) is limited to the angle interval from 45 to 90°. This limitation is attributed to the scope of the experimental study. However, on the basis of the methodology presented in this study for the uniaxial stress state, based on three uniaxial creep tests performed on three specimens oriented at angles 0, 45, and 90°, the dependence of type 4 for angles in the range of 0–90° can be determined by interpolating the results. Similarly, based on the three short-term tests for p = 0.0 MPa, the dependence of the secant modulus on the type of Equation (1) can be determined. The inclusion of the effects of lateral stress on both instantaneous and time-dependent responses requires a larger number of triaxial and short-term creep test results, depending on the predefined scope of lateral stresses relevant to the particular subject matter. In addition, the application of Equations (6) and (7) to the triaxial stress state is assumed as follows:

$$\varepsilon_1 = \varepsilon_1^e + \varepsilon_1^p + \varepsilon_1^s = \frac{\sigma_1}{E_1} + \frac{3}{2}\left(\frac{\Delta(\sigma_1 - \sigma_3)}{E_p}\right)^m\left(1 - e^{-\frac{4E_p}{3\eta_p}t}\right) + a(\sigma_1 - \sigma_3)^n t \quad (6)$$

$$\varepsilon_3 = \varepsilon_3^e + \varepsilon_3^p + \varepsilon_3^s = -\frac{\sigma_3}{E_3} - \frac{3}{2}\left(\frac{\Delta(\sigma_1 - \sigma_3)}{E_p}\right)^m\left(1 - e^{-\frac{4E_p}{3\eta_p}t}\right) - a(\sigma_1 - \sigma_3)^n t \quad (7)$$

6. Conclusions

This experimental study presents was conducted on the instantaneous and time-dependent deformation responses of Neogene marl as a representative of soft sedimentary rocks. In this study, uniaxial and triaxial short- and long-term tests were performed on marl specimens at different bedding plane orientations with respect to the loading direction.

The obtained results proved the strong effect of the inherent anisotropy on both the instantaneous and time-dependent deformation responses of soft rocks. Considering the nonlinearity of the material, the secant modulus of deformability was selected to describe the instantaneous deformation response of marl. The results of the short-term tests indicated a decreasing trend in the secant moduli of deformability in line with an increase in the angle between the loading and natural bedding planes. The interpolation of the results of the short-term tests was used to determine the parabolic dependence of the secant modulus on the angle α in the angle range of 0 to 90°.

According to the uniaxial creep test results, the velocities of the primary and secondary creeps exhibited an increasing trend with an increasing angle α. A similar trend was observed in the secondary creep velocities measured during the triaxial creep test, with the ratio between the total radial and axial deformations being practically constant throughout the test for a fixed value of the angle. The time-dependent deformation response was described using Wallner's rheological model, which was modified to include the effects of anisotropy on the marl deformation response. The dependence of the creep-related model parameters on the angle α was defined in an angle range of 45 to 90°.

The proposed model has limitations owing to the scope of the performed experiments. For further verification of the proposed model, the described methodology for the uniaxial stress state and three uniaxial creep tests on three specimens at different orientations can be used to determine the dependences of type 4 in the total angle range of 0 to 90° by means of interpolation. Similarly, the dependence of the secant modulus of Equation

(1) can be determined for the three short-term tests at a fixed lateral pressure. A greater number of triaxial, instantaneous, and creep tests must be performed to explore the effect of the lateral stress, depending on the predefined scope of the lateral stresses that are applicable a specific problem and/or primary stress state.

REFERENCES

[1] Xu, G., He, C., Chen, Z., Yang, Q.: Transversely isotropic creep behavior of phyllite and its influence on the long-term safety of the secondary lining of tunnels, Engineering Geology, 278 (2020), 105834, https://doi.org/10.1016/j.enggeo.2020.105834.

[2] Casagrande, A., Carillo, N.: Shear Failure of Anisotropic Materials, J. Boston Soc. Civ. Eng., 31 (1944) 4, pp. 78-87.

[3] Oka, F., Kimoto, S., Kobayashi, H., Adachi, T.: Anisotropic behavior of soft sedimentary rock and a constitutive model, Soils and Foundations, 42 (2002) 5, pp. 59-70.

[4] Barla, G.: Rock Anisotropy: Theory and Laboratory Testing (Chapter), Rock Mechanics, ed. L. Müller, Springer-Verlag, New York, pp. 131-169, 1972.

[5] Niandou, H., Shao, J.F., Henry, J.P., Fourmaintraux, D.: Laboratory investigation of the mechanical behaviour of tournemire Shale, Int. J. Rock Mech. Min. Sci., 34 (1997) 1, pp. 3-16.

[6] Cazacu, O., Cristescu, N.D., Shao, J.F., Henry, J.P.: A new anisotropic failure criterion for transversely isotropic solids, Mechanics of Cohesive-Frictional Materials, 3 (1998), pp. 89-103.

[7] Saroglou, H., Tsiambaos G.: A modified Hoek-Brown failure criterion for anisotropic intact rock, Int J Rock Mech Min Sci., 45 (2008), pp. 223-234.

[8] Khanlari, G., Rafiei, B., Abdilor, Y.: Evaluation of strength anisotropy and failure modes of laminated sandstones, Arab J Geosci., 8 (2015) 5, pp. 3089-3102.

[9] Singh, M., Samadhiya, N.K., Kumar, A., Kumar, V., Singh, B.: A nonlinear criterion for triaxial strength of inherently anisotropic rocks, Rock Mech Rock Eng, 48 (2015) 4, pp. 1387-1405.

[10] Aliabadian, Z., Zhao, G., Russell, A.: Failure, crack initiation and the tensile strength of transversely isotropic rock using the Brazilian test, International Journal of Rock Mechanics and Mining Sciences, 122 (2019), 104073, https://doi.org/10.1016/j.ijrmms.2019.104073.

[11] Amadei, B., Savage, W.Z., Swolfs, H.S.: Gravitational stresses in anisotropic rock masses, International Journal of Rock Mechanics and Mining Sciences & Geomechanics Abstracts, 1 (1987) 24, pp. 5-14, https://doi.org/10.1016/0148-9062(87)91227-7.

[12] Nasseri, M., Rao, K.M., Ramamurthy, T.: Anisotropic strength and deformational behavior of Himalayan schists, International Journal of Rock Mechanics and Mining Sciences, 40 (2003), pp. 3-23.

[13] Meng, L., Li, T., Liao, A. et al.: Anisotropic Mechanical Properties of Sandstone Under Unloading Confining Pressure at High Temperatures, Arab J Sci Eng, 43 (2018), pp. 5283-5294, https://doi.org/10.1007/s13369-018-3100-y.

[14] Jin, Z., Li, W., Jin, C., Hambleton, J., Cusatis, G.: Anisotropic elastic, strength, and fracture properties of Marcellus shale, International Journal of Rock Mechanics and Mining Sciences, 109 (2018), pp. 124-137.

[15] Naumann, M., Hunsche, U., Schulze, O.: Experimental investigations on anisotropy in dilatancy, failure and creep of Opalinus Clay. Phys. Chem. Earth., 8-14 (2007) 32, pp. 889-895.

[16] Sone, H., Zoback, M.D.: Mechanical Properties of Shale Gas Reservoir Rocks - Part 2: Ductile Creep, Brittle Strength, and Their Relation to the Elastic Modulus, Geophysics, 5 (2013) 78, pp. D393-D402, https://doi.org/10.1190/geo2013-0051.1.

[17] Wu, C., Chen, Q., Basack, S., Xu, R., Shi, Z.: Biaxial creep test study on the influence of structural anisotropy on rheological behavior of hard rock, J. Materials Civil. Eng., 10 (2016) 28, 04016104, https://doi.org/10.1061/(ASCE)MT.1943-5533.0001571.

[18] Khosravi, E., Ghassemi, A.: Influence of Temperature and Anisotropy on Creep Behavior of Mancos Shale, 51st U.S. Rock Mechanics/Geomechanics Symposium, 25-28 June, San Francisco, California, USA, 2017.

[19] Trzeciak, M., Sone, H., Dąbrowski, M.: Long-term creep tests and viscoelastic constitutive modeling of lower Paleozoic shales from the Baltic Basin, N Poland, International Journal of Rock Mechanics and Mining Sciences, 112 (2018), pp. 139-157.

[20] Zhang C.L., Armand G., Conil N., Laurich B.: Investigation on anisotropy of mechanical properties of Callovooxfordian claystone, Engineering Geology, 251 (2019), pp.128-45.

[21] Li, Z., Nguyen, T.S., Su ,G., Labrie, D., Barnichon, J.D.: Development of a viscoelastoplastic model for a bedded argillaceous rock from laboratory triaxial tests, Canadian Geotechnical Journal, 54 (2017), pp. 359-372, https://doi.org/10.1139/cgj-2016-0100.

[22] Wang, Z., Zong, Z., Qiao, L., Li, W.: Transversely Isotropic Creep Model for Rocks, International Journal of Geomechanics, 6 (2018) 18, (04018033), 04018033, https://doi.org/10.1061/(ASCE)GM.1943-5622.0001159.

[23] Krstić, N., Krsmanović, R., Čađenović, D., Mirković, M., Pulejković, D., Dodiković, S., Potkonjak, B.: Condition of accumulations and the age of the coal and cement marl in the Potrlice deposit-Pljevlja. Radovi Geoinstituta, 29 (1994), pp. 105-120.

[24] Pettijohn, F.J.: Sedimentary Rocks, 2nd Revised edition, Joanna Cotler Books,1957.

[25] ISRM, Commission on Standardization of Laboratory and Field Test (1981) Suggested Methods for the Rock Characterization, Testing and Monitoring, E.T. Brown (editor), Pergamon Press, Oxford, UK, 211p.

[26] Zivaljevic, S., Tomanovic, Z.: Experimental research of the effects of preconsolidation on the time-dependent deformations—creep of marl, Mechanics of Time-Dependent Materials, 19 (2015) 1, https://doi.org/10.1007/s11043-014-9250-8.

[27] Lu, Y., Wang, L.: Effect of water and temperature on short-term and creep mechanical behaviors of coal measures mudstone, Environmental Earth Sciences, 76 (2017) 17, pp. 1-15.

[28] Wallner, M.: Stability calculation concerning a room and pillar design in rock salt. In: International Congress for Geotechnics, Melbourne (1983)

[29] Tomanovic, Z.: Rheological model of soft rock based on test on marl, Int. J. Mechanics of Time-Dependent Materials, 2 (2006) 10, pp. 135-154.

[30] Tomanovic, Z.: The stress and time dependent behaviour of soft rock, GRADEVINAR, 12 (2012) 64, pp. 993-1007.